FABRICATION OF MICROFLUIDIC DEVICES WITH LOW RESOLUTION FEATURES FOR ACHIEVING HIGH RESOLUTION SEPARATION OF PARTICLES

Christopher Godfrey[1], Matt T. Hardin[1], Nick R. Harris[2], Adrian Keating[1]*

(1) School of Mechanical and Chemical Engineering, MB050, The University of Western Australia, Australia, 35 Stirling Hwy, CRAWLEY, 6009, Australia

(2) School of Electronics and Computer Science, University of Southampton,Southampton, SO17 1BJ, United Kingdom

**Email: keating@mech.uwa.edu.au*

ABSTRACT

This work describes the modeling, fabrication and testing of microfluidic devices using printed circuit boards as molds for hot embossing. The minimum feature size which could be made using these molds was 100 μm. The fabrication methods do not require clean room technologies making them inexpensive, and they provide the ability to rapidly create molds to explore high resolution microfluidic prototypes. This approach has been applied to the study of devices for the separation of particles in the sub-100 micron range using pinched flow fractionation techniques. The fabricated devices showed a measured separation of Δz = 70 μm between glass beads of 64 μm and 31μm. The smallest particles which could be separated using this fabrication technique was found to be 16 μm which agreed extremely well with modelled results.

INTRODUCTION

The separation of micron-sized particles (1-100 μm) is important in many industrial applications including point-of-care diagnostics, biochemical and biosecurity which are interested in cell separation **(**Kumar & Lykke 1984, Mattanovich & Borth 2006**)** as well as the sugar and pharmaceutical industries which are concerned with crystal growth (Iswanto 2008, Moyers and Roosseau 1987). For many of these applications, where portability, low power and disposability are important characteristics, the particle separation technique needs to be capable of not only transporting and manipulating these micron-sized particles, but must also be capable of mass production at a low cost. Microfluidic fabrication has traditionally leveraged microelectronic fabrication techniques which use silicon or glass substrates processed within a costly cleanroom environment, out of reach of many researchers (Madou 2002). The use of these microfabrication techniques is valuable for prototyping and developing novel, advanced microfluidic structures, especially where sub-micron features are required. However, as microfluidic devices are substantially larger than microelectronic devices, resulting in far fewer devices produced per wafer; the cost-benefits of such approaches may never scale as they do for microelectronics.

Alternative techniques are required to provide methods suitable for low cost, mass production. Techniques using casting, imprinting (embossing) and injection molding have been developed for microfluidic devices, solving many of the production related issues (Madou 2002, Madou *et al.* 2001). Patterned molds for these techniques are typically made using silicon or SU8 photoresist (Microchem, Massachusetts USA) using cleanroom processes. These molds have limited lifespan, requiring regular replacement. Further, silicon based molds can be easily damaged in high pressure processes, such as imprinting, which require pressures of 3-10 MPa to be applied (Merkel *et al.* 1999, Mills *et al.* 2005). As microfluidics is the basis for development of lab-on-chip technologies requiring interdisciplinary expertise from chemistry, biology, mechanical and electrical engineering, alternative methods need to be made available for prototyping microfluidic devices for these researchers.

This project's fabrication method utilises hot embossing due to its fast production, and easy setup. Printed circuit board (PCB) technology is used for the creation of inexpensive and rapidly prototyped master molds that are then hot embossed with a plastic substrate. Photosensitised copper clad printed circuit boards uses high resolution photolithography to create metal (copper) molds for subsequent embossing or casting (Keating *et al.* 2008, Merkel *et al.* (1999), Sudarsun & Ugaz 2004). However the limitation of this approach is that the microchannel widths are greater than 100 μm and the channel sidewalls are sloped and rough. Our interest is to determine how these fabrication techniques can be applied to continuous and high-resolution separation of cells and crystals, in cost sensitive industrial applications that are tolerant to these mold imperfections. There are various techniques for continuous separation of particles in a microfluidic device that could leverage this embossing approach including field-flow fractionation, pinched flow fractionation, cross-flow filtration and split-flow thin cell fractionation (Yamada *et al.* 2004). Of these, we believe only pinched flow fractionation (PFF) allows relatively low fabrication tolerances to be used to achieve relatively high resolution particle separation.

Pinched flow fractionation has been proven to effectively separate small particles (15 μm and 30 μm diameter particles), doesn't require fields to be applied and is simple to design and fabricate (Yamada *et al.* 2004). However wall roughness, in the order of the particle size, can considerably decrease the separation resolution of this particular technique because aligning particles against the channel wall is necessary for efficient particle separation (Jain & Posner 2008). To achieve smooth, high resolution features, fabrication of PFF devices has utilized complex, long cycle time methods typically based in cleanroom facilities. This work will investigate the fabrication of PFF separation devices using a rapid prototyping hot embossing technique utilizing printed circuit board molds. We will determine if the limitations of this approached can allow efficient particle separation.

FABRICATION AND DESIGN

The novel aspect of this work is the creation of stamps (molds), for use in high pressure hot embossing, based on printed circuit boards (PCB). Using these stamps for microchannel imprinting of polymers (Mills *et al.* 2005, Martynova *et al.* 1997), allows

features to be created with channel widths down to 100 μm and controllable channel depths from 17~70 μm. PCBs allow the patterning of complex designs into copper, which is backed by a strong, durable laminate (FR4) which is compatible with hot imprinting temperatures and pressures. The pattered substrates are inexpensive to create and readily available in various copper thicknesses of nominally 17 μm (½ oz-ft^2 of Cu), 35 μm (1 oz-ft^2), and 70 μm (2 oz-ft^2). This approach is similar to the work of Sadarsan & Ugaz (2004) who used etched PCBs as a mold to cast polydimethylsiloxane (PDMS) a soft elastomer. However, PDMS is subject to shrinkage, requires long setting times (or elevated temperatures) in vacuum to avoid bubbles, is porous to solvents and does not provide mechanical support. Hot embossing (imprinting) of thermoplastics allows faster fabrication of stable, biocompatible substrates such as Poly-methyl methacrylate (PMMA), making it more suitable than casting for manufacturing microfluidic devices.

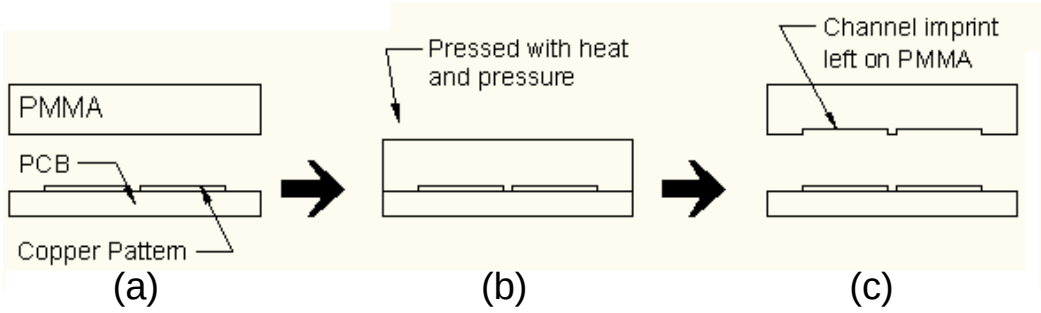

Fig. 1: Concept of the steps involved for the fabrication of microfluidic channels via imprinting; (a) alignment, (b) imprinting and (c) debonding.

Figure 1 illustrates the basic hot imprinting process. In Step (a), a patterned (etched) PCB is roughly aligned to a PMMA sheet or similar thermoplastic substrate. In Step (b), the PCB/PMMA surfaces are held in intimate contact via a set of clamps under high pressure and heated above the glass transition temperature (T_g) of the PMMA (T_g=105°C). Above this temperature, the Young's modulus of the material changes by orders of magnitude, allowing the material to reflow over the stamp, in this case a patterned PCB. Subsequently, the heat is removed, the PCB/PMMA temperature drops below the glass transition temperature and the mold and sample can be separated. At this stage the PMMA contains the channels corresponding to the copper traces on the PCB. Once completed, interconnection tubing can be bonded to the inlet and outlet ports using epoxy. In this work our PMMA substrates were 50×50 mm^2, varying in thickness from 1.5 - 3 mm.

Imprinting method

Imprinting methods have previously utilized clamps made from two flat metal plates with tightening screws in the 4 corners (Martynova *et al.* 1997). Our imprinting method utilized a hot press (Carver model #3889) with programmable heat and pressure applied at various times during imprinting. Using this system, we found that imprinting

pressures from 4-10 MPa at 120°C required a minimum of 5 minutes to create reproducible imprinted channels. A channel depth variation of 62.4±1.5 µm was measured when using the same PCB mold having 2- oz/ft^2 of copper. Mold-to-mold variation for PCBs with 2- oz/ft^2 of copper was 65±5 µm. Our imprinting conditions are consistent with previous reports by Mills *et al.* (2005) who demonstrated imprinting of PMMA samples using a clamp pressure of 3 MPa for 5 min at 120°C. Temperatures above 120°C were reported by Martynova *et al.* (1997) to cause bubbles during imprinting however we have not observed these phenomena even when imprinting at temperatures up to 130°C. The typical heating/pressure profile used on our 50×50 mm^2 samples for the remainder of this work shown is in Figure 2. Imprinting typically required around 2 hrs due to the thermal mass of the heating platens, however force air (convective) cooling helped to reduce the total time to around 80 minutes.

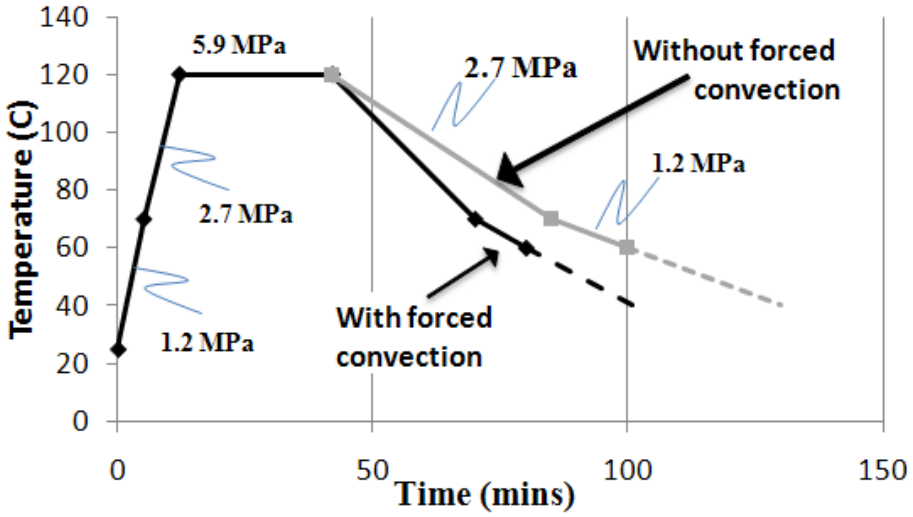

Fig. 2: Heating, pressure and time profiles used to imprint PMMA samples.

Removal from the clamps (unloading) before the temperature had cooled sufficiently resulted in warping of the imprinted sample, making it unusable. By allowing sufficient time to cool before removal from the press, the PCB mold and PMMA sample were easily debonded leaving the imprinted pattern on the PMMA. Debonding occurred at temperatures ranging from 70°C to 25°C.

Solvent bonding

While thermal imprinting is a simple method to achieve the desired channel shapes, sealing techniques using thermal bonding under pressure have been shown by Lin *et al.* (2007) to be a poor method to achieve high adhesion between PMMA layers as it leads to deformation of the channels. It is important therefore that the bonding process is performed at or near room temperature. Hui Liu *et al.* (2007) used high purity acetone to seal PMMA interfaces, which was found by Shah *et al.* (2006) to result in bond strengths of 550 kPa. However excessive exposure to acetone was found to deform and degrade the micro channels formed. We have found that by combining acetone with ethanol (which does not significantly attach the PMMA), the aggressive effects of the

acetone can be reduced, allowing defect free solvent bonding under pressure at room temperature. The optimum ratio to achieve a high strength bond with negligible channel degration was 1 part acetone to 3 parts ethanol. This solvent mixture was pipetted (roughly 200 μL) onto a blank 250 μm PMMA cover sheet (Goodfellow, UK), with the imprinted substrate pressed on top and held down with a small weight (3kg). A high strength bond was achieved after approximately 20 minutes, after which time excess solvent within the microchannels was removed by gently passing air through the channels by using a small syringe. At this stage, the fluidic channel is complete, and it is necessary to add fluidic connectors or tubes to allow fluid to enter the device.

For the testing of the devices the particles used were monodisperse glass beads supplied through Whitehouse Scientific UK. The particle diameters utilised in this work were 11.58 (± 0.19) μm, 31.33 (± 0.82) μm and 63.86 (± 0.78) μm. These particles were chosen to be representative of cells and large crystals, appropriate for our intended studies of growth rate dispersion mechanisms in crystal growth (Iswanto 2008). After considering the high density of the glass beads, glycerol was chosen as working fluid due to its high density and high viscosity; these properties resulted in a settling velocity (obtained via application of Stokes' Law) of 2 μm/s, which combined with our flow rates ranging from 0.1-1.5 ml/hr, allowed the glass beads to remain in suspension during their rapid transition down the microchannel.

Design

The pinched flow fractionation device to be investigated in this work is illustrated in Figure 3a. PFF utilizes two inflows, one with particles (Port (a), width w_a) and one without (Port (b), width w_b). As these two flows converge at a pinched segment of length L and width w_p, the particles are aligned against the sidewall by the flow coming from Port (b). The width β of the pinched wall is defined by the streamline which separated the two flows as indicated. The pinched segment then expands into a wider, outlet channel of width w_o, where the particles of different diameter (Φ_1 ,Φ_2) are spatially separated, due to the flow profile from the pinched segment. The streamline dividing the two inlet flow is subsequently measured from the wall of the broad-outlet region by χ. In all our experiments and models, both inlet channels widths were the same ($w_a = w_b$) and equal to the pinched region width w_p.

The theoretical separation of two particles which can be achieved in the outlet channel is given by Δz as:

$$\Delta z = \frac{w_o}{w_p}\frac{d_p}{2} \qquad \text{Equ.(1)}$$

where $d_p = (\Phi_2 - \Phi_1)$ is difference in the two particle diameters. By controlling the flow ratio of each inlet ($Q_b : Q_a$), the width of the pinched wall β (caused by the fluid boundary interface) can be varied. The rapid expansion at the end of the pinched section into the outlet port is associated with a large change in velocity, expanding streamlines and separation based on particle size. Yamada *et al.* (2004) suggested that the narrower the pinched section, the better the effective separation, assuming that the

punched section is not clogged with particles. Where the pinched width is less than the smallest particle size $\beta < \min[\Phi_1,\Phi_2]$ both particles are aligned to the wall and have well defined trajectories in the broad outlet region, with particle sizes defining the amount of separation. When the $\beta > \min[\Phi_1,\Phi_2]$, the particles velocities and positions as they travel in the pinched region was poorly defined, resulting in added random spatial variation in the particles as they separate in the broad outlet region.

We are interested in systems which have low fabrication tolerances which lend themselves to rapid production or low cost, volume manufacturing. In particular, due to the limitation in microchannel widths which can be achieved using PCB fabrication techniques (around 100 μm), we are looking at the operation of these devices when the pinched wall width $\beta \approx \max[\Phi_1,\Phi_2]$. Further, we have measured the surface roughness of the side walls after imprinting in our devices to be 2 μm root-mean-squared. Both the larger pinched wall width and roughness are expected to lead to suboptimal performance. However we are interested in how well our models perform under these conditions. Well performing models would allow non-ideal fabrication issues to be accounted for in subsequent designs.

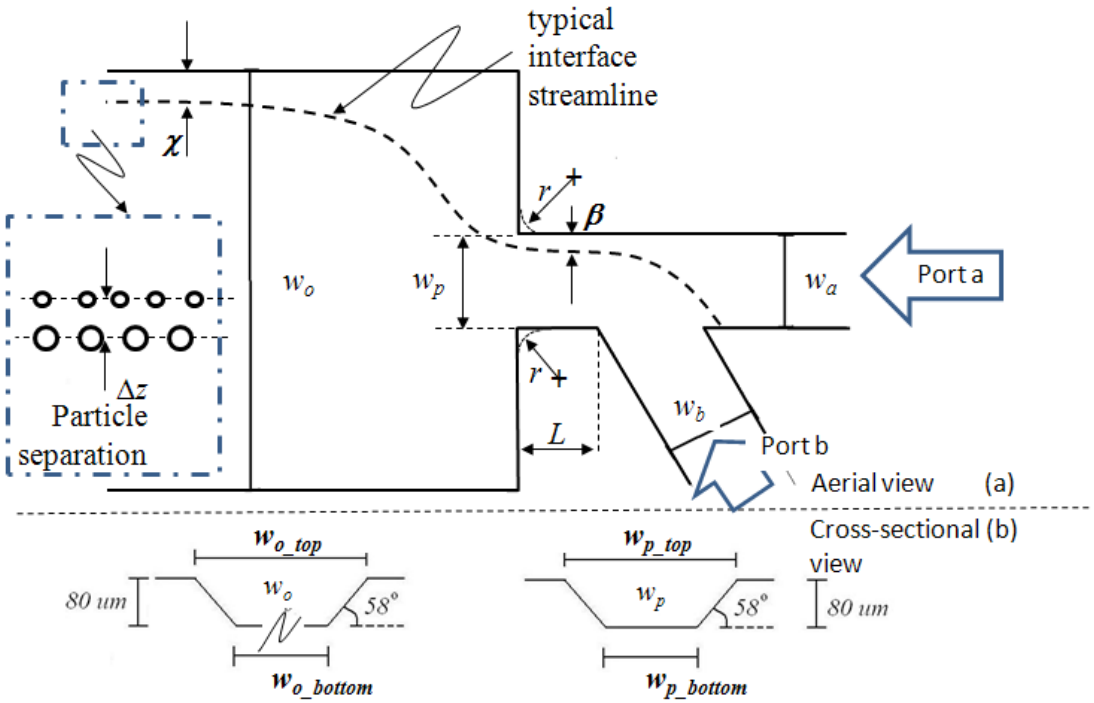

Fig. 3: Schematic representation of pinched flow fractionation (a) Plan view of the pinched flow fractional device showing the key parameters of interest and a typical stream line;(b) cross-sectional view of the channels

The etching of the PCB is a wet isotropic etch that results in a trapezoidal shaped side wall in the microchannels as illustrated in Figure 3b. The angle of the channel walls was determined to be approximately 58°. Due to this angle, there is an error in exact determination of the channel width and hence the definition of the boundary interface β. In the analysis and modelling undertaken in this work, the value of the channel width used was calculated by taking the average between the top (w_{top}) and bottom (w_{bottom}) widths, given by $w=(w_{top}+w_{bottom})/2$. The error bars in the data which follows incorporates the imaging (pixel) measurement error of ± 3 % and a side-wall error bound by $\pm (w_{top}-w_{bottom})/2 = \pm 50$ μm.

RESULTS

Figure 4a shows a measured image of the fluid flow with glycerol as the working fluid at a flow ratio Q_b/Q_a=8 with no particles in the stream. The interface in the stream was visible in these initial tests, which has been highlighted in the image. The visible interface was due to residual solvent remaining in the channels which was pushed out by the fluid during operation, but which was immiscible in the glycerol. The refractive index difference between the glycerol and the small amount of solvent allowed the interface streamline to be visible; this visible interface disappeared after continued operation; fortuitously however, it allowed initial measurement of the pinched wall distance β.

Simulations were initially performed using a computational fluid dynamics (CFD) model (ANSYS Fluent) to determine the location of the boundary interface, using models based on a device with a pinched length L = 300 μm, w_o= 1600 μm, w_p =350 μm, channel height = 80 μm. The Fluent simulations were based on a finite-element-modeling (FEM) solution to the Navier-Stokes equations in the laminar flow regime. All flow was hydrodynamic and no slip conditions were assumed at the channel walls. The simulations assumed that the side walls were straight, the particles were neutrally buoyant and there was no particle dispersion. The feature resolution in the PCB fabrication process (limited by mask underetch) resulted in a curved edge at the end of the pinched region, resulting in a finite radius of curvature, r, as schematically indicated in Figure 3a. When a radius of r = 100 μm was incorporated into the CFD model, at a flow rate of Q_b/Q_a=9 the simulations indicated the pinched region width β *increased* 17% while the streamline distance from the wall of the broad-outlet region (given by χ) *decreased* by only 2%. This result clearly indicates that feature size resolution has the greatest impact on the pinched wall width β; increased β further decreases the effectiveness of the separation in the outlet channel. Measurements of the pinched wall distance as a function of flow rate are shown in Figure 4b, along with CFD modelling results which accounted for the finite radius of curvature at the end of the pinched region. Extremely good agreement between measured and modelled values was obtained to within 10%, which approaches the systematic errors due to the imaging (pixel limited). The nominal bead size (64 μm) that we intend to separate (representative of a large crystal) is shown on the same dataset for comparison.

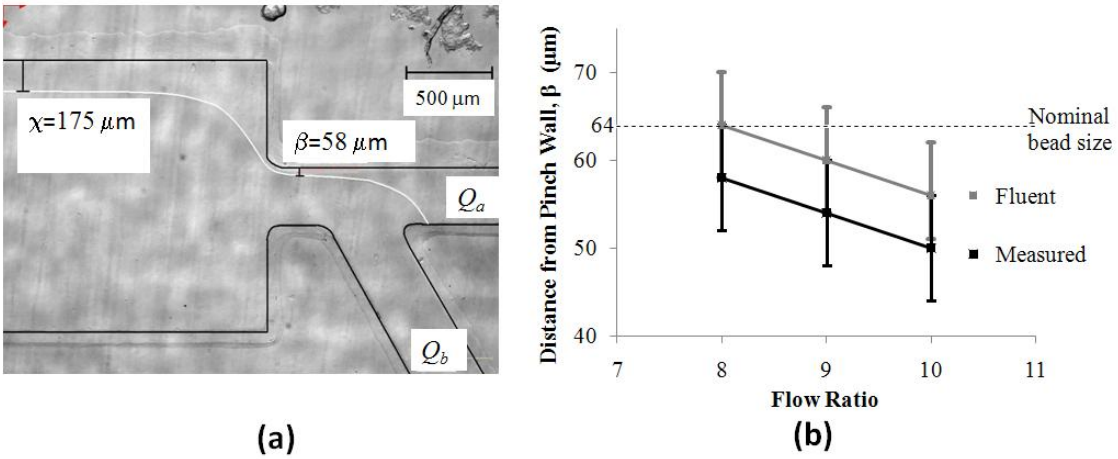

Fig. 4: (a) Image under Q_b/Q_a=8 flow conditions using glycerol illustrating key metrics of interest χ and β; (b) Measurement and CFD simulation of pinched width β.

Linearly extrapolating the measured data from 4b suggests that a flow ratio of Q_b/Q_a=15 would be required to reach a pinched wall width β~29 μm, the value required to separate our available bead size of 31 μm. Subsequently, glass beads of nominal diameter 64 μm and 31 μm were introduced into Port (a) of a device with the same characteristics as that shown in Figure 4a. The measured image is shown in Figure 5 with the white border defining the channel walls added to the image for clarity. The image was obtained using a low density of beads and overlying all the images to determine the flow paths of each bead. This permitted the no clogging condition to be met. The flow in each port for this measurement was Q_b=1.5 ml/hr and Q_a=0.1 ml/hr; this was the highest flow ratio that could be obtained before the back pressure drove the flow from Port (b) to Port (a). Both particles have been pushed firmly against the wall pinch region. There is a clear separation of the two particles at the broad outlet channel.

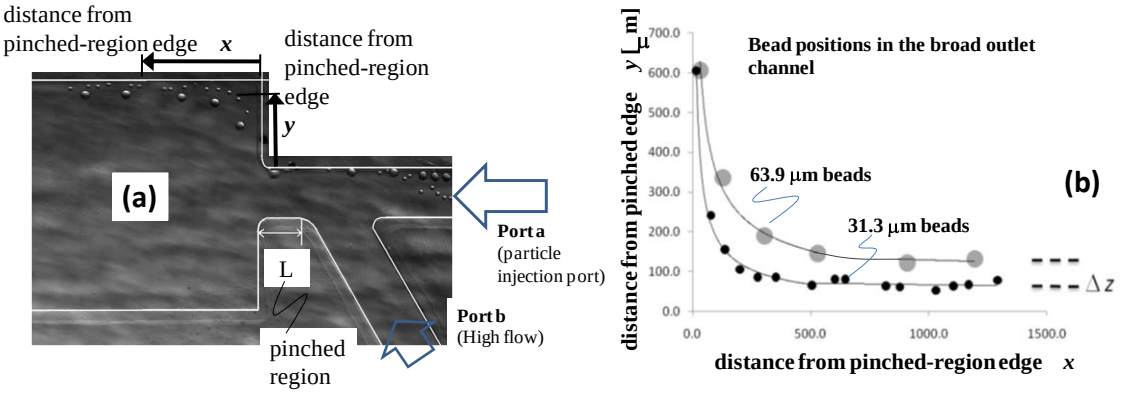

Fig. 5: (a) Image under Q_b/Q_a=9 flow conditions conditions using glycerol solution containing beads of two sizes; (b) extraction of the position data of the two beads quantifying the separation Δz.

The *x*-*y* coordinate location of each bead identified in Figure 5a was extracted and plotted in Figure 5b to highlight the degree of particle separation. The measured separation was found to be Δz = 70.3 μm. Given the parameters w_o= 1600 μm, w_p =350 μm and the difference in bead size of Δd_p= (63.86-31.33) = 32.6 ± 1.1 mm, we obtain a theoretical value of Δz= 75 μm using equation (1). The measured and the theoretical value for the particle separation (Δz) agreed extremely well, to within 6.3%. This result combined with the excellent agreement in the pinched region width β shown in Figure 4b, implies that the sidewall angle has little effect on the particle separation. This is extremely interesting given that the sloped side walls (±50 μm.) in the pinched region width (w_p) represents almost a 30% change in the width. These result show that by using the average channel width to analyse these systems, side wall slope has negligible effect on the calculated pinched region width β and the theoretical particle separation Δz; these are both critical parameters in designing and analysing pinched flow fractionation systems.

Based on this evidence, we wanted a design guide for particle separation and to determine the smallest particles which could be separated using traditional water based carrier fluids. For this reason, in the following tests we used water as the working fluid, with the beads at Port (a) replaced by a dye. This allowed clear visualization of the pinched region width β and the theoretical particle separation Δz. Figure 6a shows the boundary interface location in the pinched region for two different outlet regions, w_o=1000 μm and w_o=2500 μm. Again, there is a very strong correlation between the measured results for β and the simulations. The maximum difference between the simulated and measured β results (for w_o=1000 μm) was Δβ = 2 μm, which is well

within the estimated error. The smallest value for β was 16 μm; given the need to have $\beta < \min[\Phi_1,\Phi_2]$, this suggests this device could be used for separating particles of 16 μm diameter and larger. For the 100 μm minimum feature size we are using and the relatively large channel width used (for w_o=350 μm), this result is extremely encouraging for achieving high performance particle separation using low resolution, low cost manufacturing of microfluidic devices. Based on these measurements, at a flow rate of Q_a = 0.1 mL/hr and assuming particle diameters in the order of β, the number of particles per second that could be separated ranges from 160 s^{-1} (Q_b/Q_a = 4) to 990 s^{-1} (Q_b/Q_a = 15).

Figure 6b similarly shows the measured and simulated locations of the boundary interface location (χ) at the outlet. The comparison shows these values are almost identical, however, the simulated results start to differ towards higher flow ratios (higher than theoretical). These 2nd order variations may be due to non-linearity in the models or imperfections in the physical system and are currently under investigation.

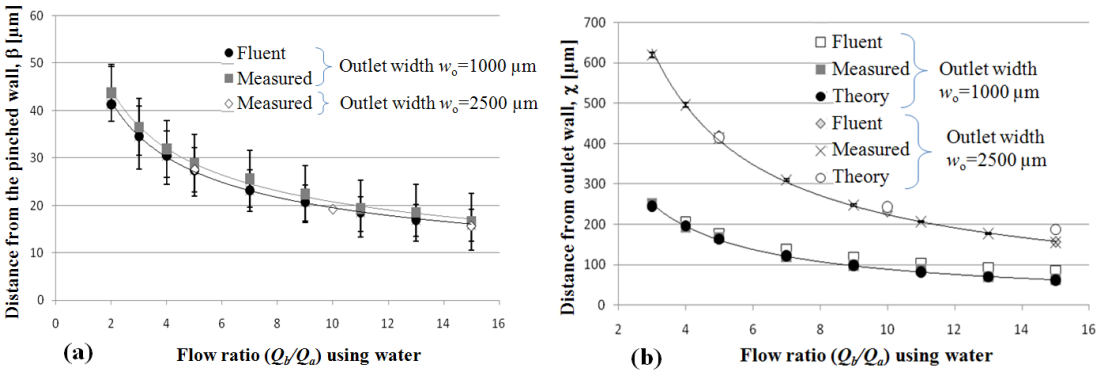

Fig. 6: Simulated and measured results for two different outlet widths using water showing (a) pinched region boundary interface location β and (b) outlet boundary interface location χ.

CONCLUSIONS

This project has demonstrated that a simple, embossing fabrication technique can produce microfludic devices whose performance for pinched flow fractionation agrees well with that predicted by theory and models. This process enables microfluidic particle separation devices to be rapidly created using low cost materials, enabling exploration of novel structures by researchers with access to relatively common tool sets. The simulations suggest that high performance can be obtained with low resolution and inexpensive molds and that the current approach of using expensive cleanroom toolset could be largely eliminated if the systems under consideration are well modelled and understood. Interestingly, for pinched flow fractionation systems, improving the resolution of the channels to achieve straighter channel corners and edges would only slightly reduce the required ratio of inlet flows to achieve particle separation. The results indicate that the feature resolution for PCB molds of around 100 μm should allow particles down to 16 μm to be separated effectively. This is more than adequate to investigate many cells and crystal growth mechanisms. Methods to further reduce the channel dimensions and improve the design rules which would guide the efficient separation of even smaller particle sizes are currently under investigation.

REFERENCES

Hui Liu, R., Yang, J., Lenigk, R., Bonanno, J. and Grodzinski, P., 2004, 'Self-Contained, Fully Integrated Biochip for Sample Preparation, Polymerase Chain Reaction Amplification, and DNA Microarray Detection,' Anal. Chem. 76, 1824-1831

Iswanto, N., 2008,'Growth Rate Dispersion of Sucrose Crystals', PhD Thesis, School of Engineering, The University of Queensland, Australia

Keating, A.J., Gager,M., Clarke, D. 2008 'Rapid prototyping of microfluidic devices using imprinting: application to microvalves and micropumps', Proceedings Vol. 7269, Micro- and Nanotechnology: Materials, Processes, Packaging, and Systems IV, 72690X

Kumar, R. K, Lykke, A. W. J., 1984 'Cell Separation: A Review', Pathology (1984), 16, pp. 53-62

Lin, C.-H., Chao, C.-H., Lan, C.-W., 2007, 'Low azeotropic solvent for bonding of PMMA microfluidic devices', Sensors and Actuators B 121, 698–705

Madou, M. J., 2002, 'Fundamentas of microfabrication -- The science of miniaturization', CRC-Press, 2nd Ed

Madou, M. J., Lee, L. J., Koelling, K. W., Daunert, S., Lai, S., Koh, C. G., Juang, Y.J., Yu, L. and. Lu, Y., 2001, 'Design and Fabrication of Polymer Microfluidic Platforms for Biomedical Applications,', ANTEC, 2534-2538

Martynova, L., Locascio, L.E., Gaitan, M., Kramer, G. W., Christen, R. G., & MacCrehen, W. A., 1997, 'Fabrication of plastic microfluid channels by imprinting method', Analytical chemistry 69(23), 4783-4789

Mattanovich, D, Borth, N., 2006 'Applications of cell sorting in biotechnology', Microbial Cell Factories, 5:12, doi:10.1186/1475-2859-5-12

Merkel, T, Graeber, M & Pagel, L 1999, 'A New Technology for Fluidic Microsystems based on PCB Technology', *Sensors and Actuators*, vol. 77, pp. 98-105

Mills, C.A., Martinez, E., Bessueille, F., Villanueva, G., Bausells, J., Samitier, J., Errachid, A., 2005, 'Production of structures for microfluidics using polymer imprint techniques' ,Microelectronic Engineering 78–79, 695–700

Moyers, C.G. Jr, Roosseau, R. W., 1987, Crystallization Operations, in 'Handbook of Separation Process Technology', John Wiley & Sons, Inc, ISBN 0-471-89558-X

Shah, J.J., Geist, J., Locascio, L.E., Gaitan, M., Rao, M. V., Vreeland, W. N., 2006, 'Capillarity Induced Solvent-Actuated Bonding of Polymeric Microfluidic Devices', Anal. Chem.78(10), 3348 –3353

Sudarsun, AP & Ugaz, VM 2004, 'Printed Circuit Technology for Fabrication of Plastic-Based Microfluidic Devices', *Analytical Chemistry*, vol. 76, no. 11, pp. 3229-3235